Supplementary material

Roaming-Controlled Formation of Dimethyl Ether and Methanol: Role of Nonequilibrium Dynamics and Integrability

Toshiaki Matsubara*

Department of Chemistry, Faculty of Science, Kanagawa University,
3-27-1, Rokkakubashi, Kanagawa-ku, Yokohama 221-8686, Japan

Note S1. Crossover Temperature and the Role of Tunneling

Tunneling effects are often considered in hydrogen-transfer reactions due to the small mass of hydrogen atoms, which facilitates quantum mechanical barrier penetration. This contribution becomes particularly significant at low temperatures, where thermal activation is suppressed. To evaluate the potential contribution of tunneling in the present reactions, we employ the concept of the crossover temperature (T_c), which approximates the temperature below which tunneling becomes more probable than classical, over-the-barrier thermal activation. *T*c provides a convenient diagnostic for estimating the importance of quantum effects relative to thermal activation.

The crossover temperature is calculated using the semiclassical expression,[1] which balances thermal and quantum contributions to the rate:

$$T_c = \frac{\hbar|\omega^{\ddagger}|\Delta {E_o}^{\ddagger}/k_B}{2\pi\Delta {E_o}^{\ddagger} - \hbar|\omega^{\ddagger}|\ln(2)} \qquad \text{(S1)}$$

Here, $\omega^{\ddagger} = 2\pi\nu^{\ddagger}$, where $\nu^{\ddagger}$ is the magnitude of the imaginary frequency at the transition state, and $\Delta {E_o}^{\ddagger}$ is the zero-point energy (ZPE)-corrected energy barrier. $\hbar = h/2\pi$ is the reduced Planck's constant, and k_B is the Boltzmann's constant. Harmonic frequencies were scaled by a factor of 0.971,[2] and all data were obtained at the M06-2X/aug-cc-pVTZ level of theory.

Cationic Pathway:

For the cationic pathways leading to dimethyl ether (DME) and methanol (MeOH), the ZPE-corrected energy barriers are substantial—31.4 kcal/mol and 32.7 kcal/mol, respectively. The corresponding transition-state imaginary frequencies are 1816.3 cm^{-1} (DME) and 1700.9 cm^{-1} (MeOH), yielding calculated T_c values of 424 K and 396 K, respectively. These relatively high crossover temperatures indicate that tunneling becomes significant only at temperatures far below them, such as those found in interstellar environments (10–100 K). However, the large barrier heights fundamentally limit the reaction's probability via either tunneling or thermal pathways under such cold conditions. More importantly, under the present simulation conditions, the system acquires substantial excess internal energy (~90 kcal/mol) through an ionization event. This excess energy greatly exceeds the activation barriers, resulting in strongly nonequilibrium conditions. Under such circumstances, thermal activation becomes the dominant mechanism, even at low external temperatures, rendering tunneling effects negligible. Thus, while the calculated T_c suggests that tunneling is theoretically possible, its actual contribution under the current conditions is likely minimal.

Neutral Pathway:

In contrast, the neutral pathways exhibit much lower ZPE-corrected energy barriers: 1.7 kcal/mol (DME) and 1.6 kcal/mol (MeOH), with imaginary frequencies of 850.4 cm^{-1} and 720.1 cm^{-1}, respectively. These values yield T_c estimates of 231 K and 192 K, which imply that tunneling could become significant at low temperatures (10–100 K) relevant to astrochemical environments. However, the relatively low barriers suggest that thermal activation remains efficient and dominant across a wide temperature range extending down to very low temperatures. Moreover, in the neutral simulations, the system is still initiated with significant excess energy (~20 kcal/mol), which further enhances the efficiency of thermally driven transitions. As a result, thermal activation remains the dominant mechanism rather than tunneling, even under such low-temperature conditions.

Conclusion and Outlook:

Tunneling contributions, as estimated via the crossover temperature, did not significantly influence the reaction outcome and were found to be negligible especially in the presence of substantial excess energy. Accordingly, the present study focuses on thermally activated dynamics under nonequilibrium conditions, where tunneling is expected to play a minimal role.

It should be noted, however, that the expression for T_c in eqn (S1) is derived under the assumption of a canonical thermal energy distribution and does not explicitly account for nonequilibrium excitation, such as that introduced by ionization. A natural extension of this work will be to incorporate excess internal energy into the estimation of T_c, enabling a more comprehensive description of reaction dynamics in astrochemical and other high-energy environments.

Note S2. Time-Resolved Analysis of the Overlap Integral

To assess the degree of electronic independence between fragments during the roaming period, we calculated the overlap integral

$$S = \int \psi_A^*(r)\psi_B(r)dr \qquad \text{(S2)}$$

between the CH_2 and CH_3OH fragments along representative trajectories. In this analysis, we primarily focus on the absolute value $|S|$, which serves as a robust measure of the spatial overlap between fragment-localized wavefunctions. A near-zero value of $|S|$ indicates minimal orbital overlap, consistent with spatial separation or dynamical decoupling of the fragments. The representative trajectories for dimethyl ether and ethanol formation presented in the main text were used for the analyses.

For both dimethyl ether and ethanol formation pathways, $|S|$ remains close to zero during the roaming period, suggesting that CH_3OH and CH_2 behave as dynamically and electronically

independent entities. Fig. S1a,b show the time evolution of the total orbital overlap $\sum|S|$ between the two fragments for dimethyl ether and ethanol formations, respectively. The trends in $\sum|S|$ closely follow those of the interaction energy (Fig. 8d for dimethyl ether formation and Fig. 12d for ethanol formation), supporting its use as an auxiliary indicator of fragment independence in quasi-integrable regimes.

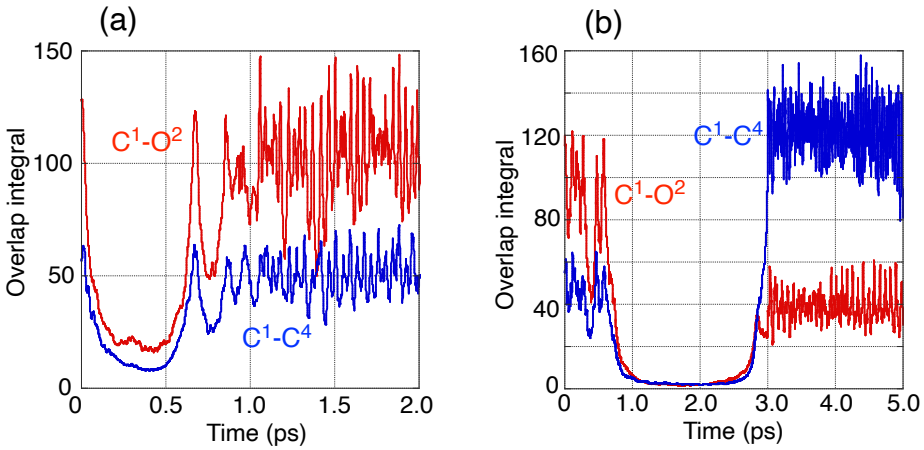

Fig. S1 Time-dependent overlap integrals for C^1–O^2 and C^1–C^4 in the isomerization: (a) from the CH_3OH–CH_2 adduct ($C^4H_3O^2HC^1H_2$) to the dimethyl ether product ($C^4H_3O^2C^1H_3$), and (b) from the CH_3OH–CH_2 adduct ($C^4H_3O^2HC^1H_2$) to the ethanol product ($C^1H_3C^4H_2O^2H$), obtained from molecular dynamics simulations.

Note S3. Time-Resolved Analysis of the Bond Population

The bond population between CH_2 and CH_3OH was also monitored during the roaming period as a measure of covalent bonding character. In both the dimethyl ether and ethanol formation pathways, the bond population rapidly decreases to near zero and remain negligible throughout the roaming period (Fig. S2a,b), indicating the absence of significant bonding interaction between the fragments. These results are consistent with the near-zero overlap integral and further support the picture of electronic decoupling during the roaming stage.

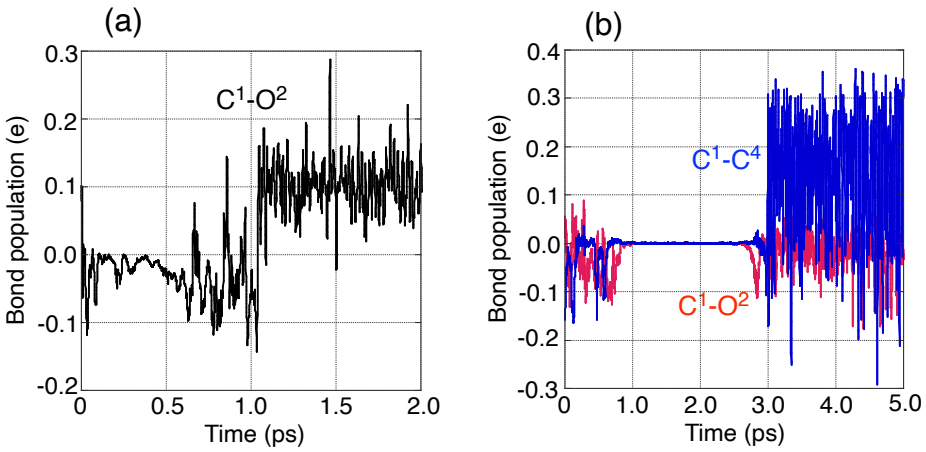

Fig. S2 Time-dependent bond populations: (a) for C^1–O^2 in the isomerization from the CH_3OH–CH_2 adduct ($C^4H_3O^2HC^1H_2$) to the dimethyl ether product ($C^4H_3O^2C^1H_3$), and (b) for C^1–O^2 and C^1–C^4 in the isomerization from the CH_3OH–CH_2 adduct ($C^4H_3O^2HC^1H_2$) to the ethanol product ($C^1H_3C^4H_2O^2H$), obtained from molecular dynamics simulations.

Note S4. Potential and Kinetic Energies and NBO Charges

As shown by Fig. S3a, during the integrable period, the potential energy of the combined CH_3OH + CH_2 system increases, while the kinetic energy decreases, consistent with the formation and persistence of a distinct, energetically decoupled state. This trend in energy changes arises as kinetic energy is injected into the bonding interaction between CH_2 and CH_3OH within this state. In addition, during the roaming period, both fragments remain neutral in charge (Fig. S3b), further supporting their mutual independence. In contrast, when the system is not in a roaming state, charge is exchanged between CH_3OH and CH_2, indicating that, like energy flow, chemical bonding involves charge transfer—essentially, the flow of electrons.

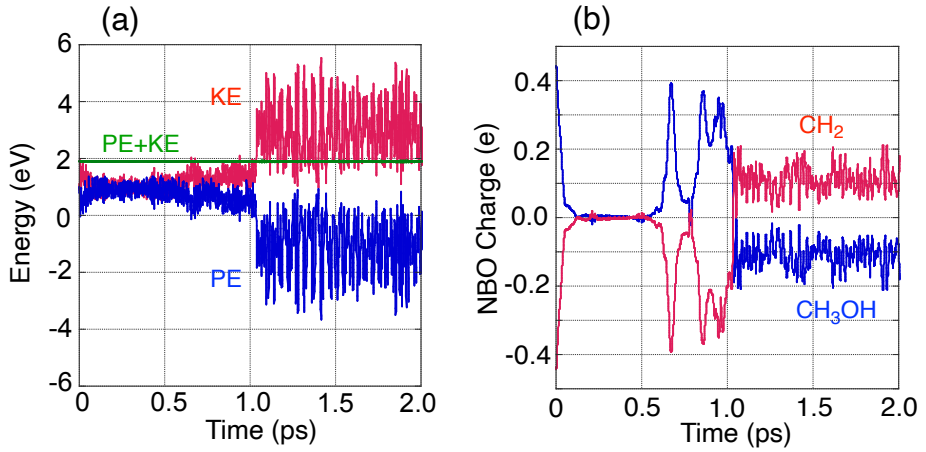

Fig. S3 Potential energy (PE), kinetic energy (KE), and their sum for the entire molecule (a); and natural bond orbital (NBO) charges of the fragments (b) as functions of time in the isomerization of CH_3OHCH_2 to CH_3OCH_3 during molecular dynamics simulation.

Note S5. Potential and Kinetic Energies and NBO Charges

Fig. S4a shows that both fragments, CH_3OH and CH_2, remain neutral in charge and no net charge transfer is observed, throughout the roaming period. In addition, the fluctuation profile of the molecular PE and KE changes during this period due to the quasi-integrable state (Fig. S4b).

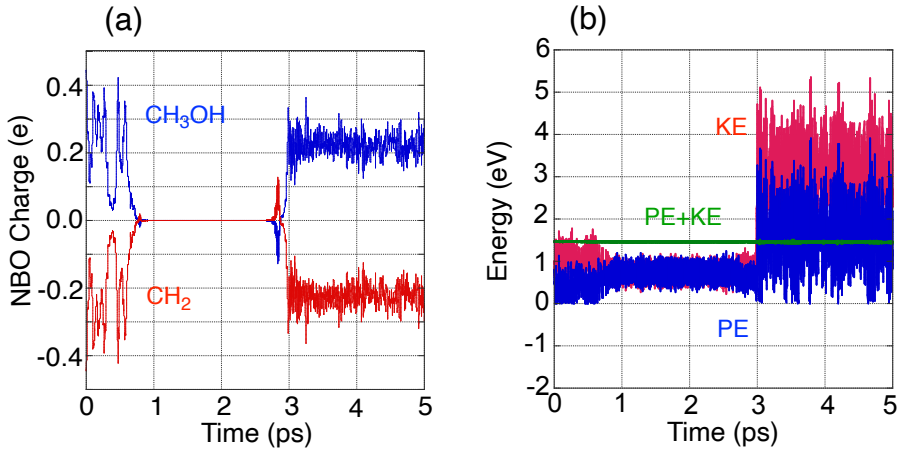

Fig. S4 Natural bond orbital (NBO) charges of the fragments (a); and potential energy (PE), kinetic energy (KE), and their sum for the entire molecule (b) as functions of time in the isomerization of CH_3OHCH_2 to CH_3CH_2OH during molecular dynamics simulation.

Note S6. Potential and Kinetic Energies and NBO Charges

Fig. S5a shows that both fragments, CH_2 and H_2O, remain neutral in charge and no net charge transfer is observed throughout the roaming period. In addition, Fig. S5b shows the changes in the fluctuation profile of the molecular PE and KE during the same period.

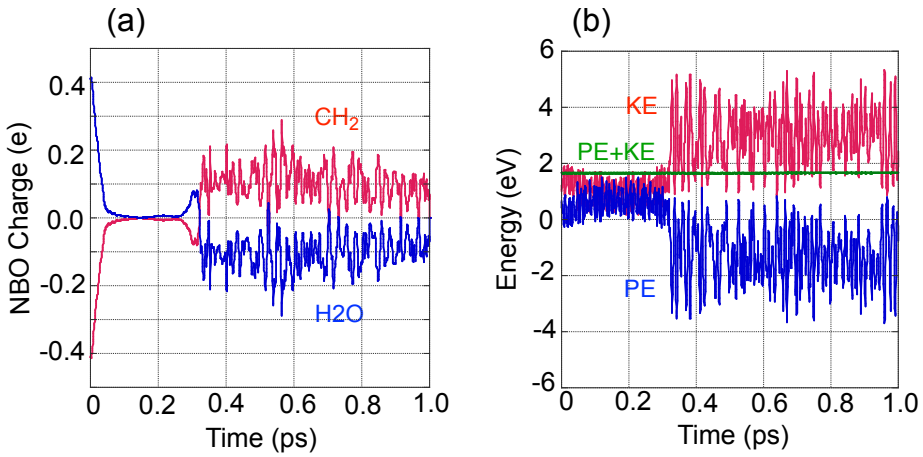

Fig. S5 Natural bond orbital (NBO) charges of the fragments (a); potential energy (PE), kinetic energy (KE), and their sum for the entire molecule (b) as functions of time in the isomerization of CH_2OH_2 to CH_3OH during molecular dynamics simulation.

Supporting Information References

1 J. T. Fermann and S. Auerbach, *J. Chem. Phys.*, 2000, **112**, 6787–6794.

2 I. M. Alecu, J. Zheng, Y. Zhao and D. G. Truhlar, *J. Chem. Theory Comput.*, 2010, **6**, 2872−2887.

Table S1 Patterns of motion for all normal modes of **TS2** and their corresponding vibrational frequencies at the M06-2X/aug-cc-pVTZ level

Normal mode No.	Vibrational frequency (cm^{-1})	Pattern of motion
1	875.8*i*	H migration
2	172.2	CH_3 rotation around C–O
3	281.0	CH_2 rotation around C–O
4	331.6	COC bending
5	471.7	C(CH_2)–O stretching
6	1023.8	CH_2 twisting
7	1095.5	C(CH_3)–O stretching
8	1134.2	CH_3 wagging
9	1147.7	CH_2 wagging
10	1212.8	CH_3 wagging
11	1340.6	HOC bending
12	1419.8	HCH bending
13	1472.7	Umbrella motion of three H atoms
14	1497.6	HCH bending
15	1502.3	HCH bending
16	2921.8	O–H stretching
17	3054.5	C–H stretching
18	3059.1	C–H stretching
19	3133.5	C–H stretching
20	3147.4	C–H stretching
21	3155.8	C–H stretching

Table S2 Patterns of motion for all normal modes of **TS4** and their corresponding vibrational frequencies at the M06-2X/aug-cc-pVTZ level

Normal mode No.	Vibrational frequency (cm^{-1})	Pattern of motion
1	741.6*i*	H migration
2	406.3	C–O stretching
3	430.9	CH_2 and OH_2 rotation around C–O
4	782.3	CH_2 and OH_2 twisting
5	1061.8	CH_2 and OH_2 twisting
6	1138.7	CH_2 and OH_2 wagging
7	1413.5	HCH bending
8	1508.7	HOH bending
9	2878.2	O–H stretching
10	3066.4	C–H stretching
11	3151.6	C–H stretching
12	3864.4	O–H stretching

Cartesian coordinates (in Å)

1

C 1.130591 -0.610583 -0.000219
O 0.683709 0.733207 -0.000475
H 0.240428 -1.236536 -0.004847
H 1.723616 -0.842753 -0.887992
H 1.715715 -0.845052 0.892167
H 1.444756 1.316577 0.006068
C -2.244112 -0.154252 -0.000529
H -1.953928 0.169313 -0.984290
H -1.959136 0.161804 0.987180

2

C 1.221432 -0.220485 0.047084
O -0.087364 0.467834 -0.139441
H 1.207151 -1.044257 -0.658065
H 1.976692 0.513415 -0.211665
H 1.279116 -0.549980 1.079543
H -0.116216 1.359499 0.249481
C -1.269956 -0.289205 0.098652
H -1.197280 -1.282161 -0.312896
H -2.159407 0.318954 0.094715

3

O 0.000012 -0.498138 0.000100
C 1.218869 0.186085 0.005486
C -1.218867 0.186119 -0.005392
H -1.095733 1.261107 -0.091988
H -1.721600 -0.114578 0.931558
H -1.818734 -0.270718 -0.804925
H 1.820334 -0.273001 0.802414
H 1.719763 -0.111799 -0.933459
H 1.095863 1.260860 0.095038

4

C -1.169201 0.271985 0.023795
O -0.016491 -0.563558 -0.147882
H -1.192594 0.934237 -0.835427
H -2.059246 -0.352022 0.044453
H -1.054732 0.848871 0.940718
H 0.023557 -1.189707 0.582721
C 1.374338 0.292382 0.195070
H 1.139545 1.177545 -0.415686
H 2.044577 -0.296662 -0.446915

5

O 0.000034 -0.591124 -0.000019
C 1.162806 0.195340 0.000016
C -1.162855 0.195322 0.000001
H -2.018182 -0.475977 0.000736
H -1.206986 0.834726 0.889001
H -1.207637 0.833783 -0.889670
H 1.207641 0.833905 0.889544
H 2.018022 -0.476087 -0.000502
H 1.207164 0.834675 -0.889059

6

O 1.513925 0.034599 -0.096662
H 1.723108 -0.284978 0.783322
C -1.729309 -0.015255 0.092421
H -2.012477 -0.952290 -0.353847
H -1.997916 1.013145 -0.072188
H 0.551739 0.038863 -0.138513

7

O 0.634869 -0.000074 -0.082669
H 1.094896 0.808986 0.213467
C -0.803256 -0.000100 0.091957
H -1.225062 -0.958234 -0.161434
H -1.224408 0.959020 -0.158870
H 1.095159 -0.808583 0.216450

8

C -0.626654 0.072588 0.000136
H -1.054345 -0.580900 -0.817018
H -0.968603 1.101231 0.000381
H -1.054774 -0.582204 0.815795
O 0.699233 -0.132625 0.000022
H 1.243781 0.687343 -0.000147

9

C -0.959321 -0.000000 0.192711
H -1.176132 0.859542 -0.459500
H -1.176132 -0.859542 -0.459500
O 0.758392 -0.000000 -0.128990
H 1.020529 -0.764450 0.397325
H 1.020529 0.764450 0.397325

10

C -0.663209 0.020601 0.000006
H -1.083051 -0.982512 -0.000178
H -1.020124 0.544880 -0.889911
H -1.020070 0.544760 0.890057
O 0.744387 -0.122252 0.000021
H 1.147400 0.747278 -0.000170

TS1

O -0.064045 -0.525488 -0.076662
C 1.229951 0.187482 -0.006195
C -1.242086 0.255202 0.006678
H 1.356435 0.646771 -0.983204
H 1.968268 -0.582063 0.183797
H 1.185908 0.926602 0.790355
H -1.116087 1.328477 0.057143
H -2.109915 -0.256172 -0.388440
H -0.699435 -0.515818 0.950748

TS2

O -0.053612 -0.606590 0.098178
C -1.183705 0.255081 0.002344
C 1.399701 0.255320 -0.133853
H -1.243360 0.825936 0.926855
H -2.076156 -0.353659 -0.124849
H -1.065084 0.937102 -0.840958
H 1.095133 1.254885 0.185800
H 1.992160 -0.192218 0.664912
H 0.430230 -0.681736 -0.808132

TS3

C -0.731498 0.035490 -0.006808
H -1.245273 -0.863498 0.306623
H -1.134545 1.038468 0.023442
O 0.686822 -0.105718 0.083696
H 1.159204 0.753587 0.027730
H 0.115024 -0.295751 -0.986519

TS4

C -0.953200 -0.007881 -0.135316
H -1.217667 -0.721844 0.646093
H -1.139247 0.993698 0.260801
O 0.821503 -0.093952 0.085664
H 0.362037 -0.286618 -0.818082
H 1.142056 0.813664 0.037769